**Per. Mineral. (2006), *75*, 2-3, 11-24** http://go.to/permin

**PERIODICO di MINERALOGIA**
*established in 1930*

***An International Journal of***
*MINERALOGY, CRYSTALLOGRAPHY, GEOCHEMISTRY, ORE DEPOSITS, PETROLOGY, VOLCANOLOGY*
and applied topics on *Environment*, *Archaeometry* and *Cultural Heritage*

# Determination of the origin of unusual glass with metallic spherule inclusions found in the area between Inzingkofen and Sigmaringen (Bavaria, Germany), South-West of the Steinheim-Ries craters

Matteo Ardit,[1] Anna Maria Fioretti,[2*] Gianmario Molin,[3] Emilio Ramous[4] and Ulf-Christian Bauer[5]

[1] Centro di Ateneo per i Musei, via Orto Botanico, 15 – 35122 Padova (Italy)
[2] Istituto Geoscienze e Georisorse - CNR, c.so Garibaldi, 37 – 35137 Padova (Italy)
[3] Dipartimento di Mineralogia e Petrologia, Università di Padova, c.so Garibaldi, 37 – 35137 Padova (Italy)
[4] Dipartimento di Innovazione Meccanica e Gestionale, Università di Padova, via Venezia, 1 – 35139 Padova (Italy)
[5] Seestrasse, 46a – 83727 Schliarsee (Germany)

Abstract. — This paper reports the characteristics of a suite of pale green glass fragments and their metallic spherule inclusions (5 to 400 μm) found over a relatively wide area between Inzigkofen and Sigmaringen (Bavaria, Germany), about 150 km SW of the Steinheim-Ries impact craters. The distribution area of these glasses and their close macroscopic similarity (apart from the spherules) with moldavite suggested us that they may shed new light on the nature of the binary asteroid which caused the Steinheim-Ries impact craters. However, our petrographic and chemical data rule out an extra-terrestrial origin. Metallographic microstructure, lack of Ni and high P contents (up to 9 wt.%) reveal the metallic inclusions as cast iron spherules. The chemical composition of the host glass consistently differs from both moldavite and suevite compositions. Our data indicate that the investigated samples are by-products of metallurgic activity. This conclusion is consistent with the presence in the Sigmaringen area of important cast iron furnaces which have been operating since the 18th century.

Key Words: *slag, cast iron, metallic spherules, moldavite, Ries crater.*

* Corresponding author, E-mail: anna.fioretti@igg.cnr.it

Riassunto. — In questo lavoro vengono studiati diversi frammenti di vetro verde chiaro aventi la particolarità di contenere inclusioni di sferule metalliche (di dimensioni variabili tra 5 e 400 μm), ritrovati in un'area relativamente vasta tra Inzigkofen e Sigmaringen (Baviera, Germania), a ~150 km SW dai crateri di impatto di Steinheim-Ries. La distribuzione areale di questi vetri e la loro stretta somiglianza macroscopica con le moldaviti (ad eccezione che per le sferule) ci suggerirono che essi potessero contribuire a chiarire la natura dell'asteroide binario che generò i crateri di Steinheim-Ries. I nostri dati chimici e petrografici escludono tuttavia un'origine extraterrestre dei vetri. La microstruttura metallografica, l'assenza di Ni e l'elevato contenuto in P (anche superiore al 9 wt.%) indicano che le inclusioni metalliche sono sferule di ghisa. La composizione chimica dei vetri in studio differisce sistematicamente da quella delle moldaviti e della suevite. I nostri dati indicano che i campioni studiati rappresentano pertanto un sottoprodotto di attività siderurgica. Questa conclusione è avallata dal fatto che nelle vicinanze di Sigmaringen sono attivi altoforni operanti sin dagli inizi del XVIII secolo.

Parole Chiave: *scoria di fusione, ghisa, sferule metalliche, moldavite e cratere di Ries.*

## Introduction

In the early 1960s, one of the authors (UCB) found several fragments of pale green glass with metallic spherule inclusions (5 to 400 μm) in a relatively wide area between Inzigkofen and Sigmaringen, near the Danube river, about 150 km SW of the Steinheim-Ries impact craters (Fig. 1). Except for their inclusions, macroscopically the glass closely resembles moldavite (see later), a group of tektites which were generated during the Steinheim-Ries impact event. Although the area where the glass fragments were found is exactly opposite (with respect to the Steinheim-Ries craters) the moldavite distribution area (Fig. 1), the close similarity of the new glasses with tektite prevented us from excluding *a priori* that these materials were totally unrelated.

A wide variety of distinctive rock types (tektites, glass, breccias, melts, shock-metamorphosed target rocks) are actually produced during impacts. Glass and melted meteoritic metal spherules, formed as a consequence of terrestrial impacts, have been found in association with young, well-preserved craters (e.g. Wabar, Saudi Arabia). However, these spherules are not commonly observed, perhaps because such ejected molten particles do not survive the disruptive effects of the atmosphere, or because they are quickly destroyed by weathering and erosion (French, 1998). One of the main interests in studying these materials is that they may provide information on the nature and composition of the impactor.

The Steinheim-Ries craters originated about 14.34 Ma ago (Laurenzi *et al.*, 2003) in an area where minimal later erosion allowed the

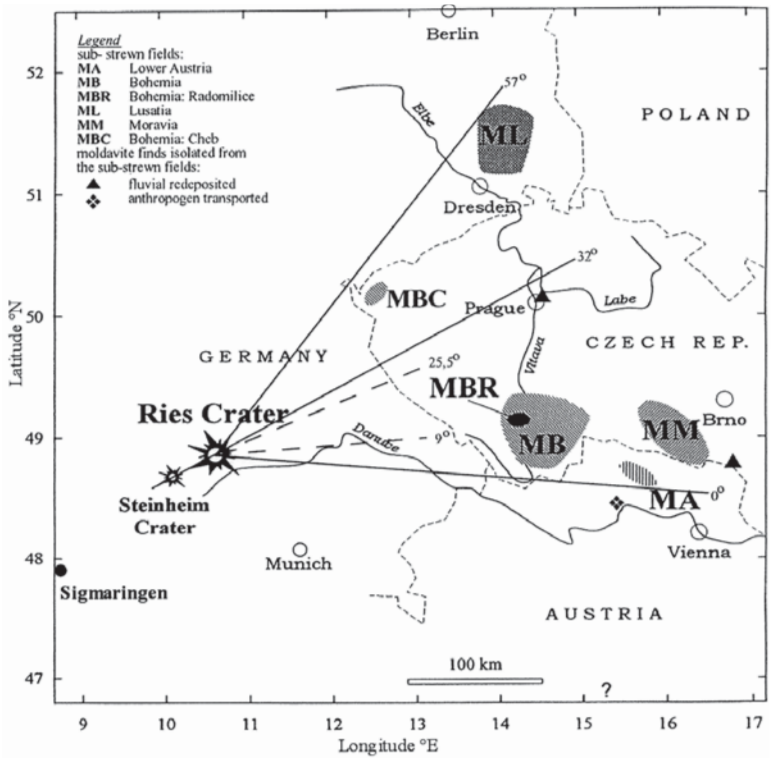


Fig. 1 – Map of Central Europe, showing Ries and Steinheim craters and moldavite strewn field (modified after Lange, 1996). Dashed lines (9 to 25.5°) define fan within which coherent melt patches are observed on inner slope of Ries crater rim. Moldavite strewn field extends about 450 km from the centre of the Ries crater to ENE forming a fan with an angle of about 57° (Stöffler *et al*., 2002).

preservation of the impact products. The target rocks consist of a sequence of sedimentary rocks (limestone, shale, sandstone) (Tab. 1) underlain by crystalline rocks (gneiss, granite, and metabasite) (Hüttner & Schmidt-Kaler, 1999; Stöffler *et al*., 2002). The impact produced melting of distinct target rocks generating moldavite, suevite (a polymict breccia with clastic matrix and melts), and a variety of breccias and glass (Engelhardt, 1997; Osinski, 2003).

Moldavites have a typical green colour and vary in size from less to 1 mm (micro-tektites) to about 20 cm. They have persilicic composition that is constant, and characteristic for the strewn field (French, 1998). To the best of our knowledge, no metallic spherules have been reported within moldavite.

The fall-out suevite is an impact breccia characterised by the presence of glass fragments (Stoffler, 1974; Engelhardt, 1997). Four glass types are distinguished within suevite by Osinski (2003) on the basis of their composition and microtextures. They show wide ranges in $SiO_2$ (50 to 100 wt.%), $Al_2O_3$ (up to 21 wt.%), high CaO (up to 7 wt.%), and $H_2O$ (up to 17 wt.%), consistent with the melting of distinct protoliths.

In spite of the great amount of melted material produced during the Steinheim-Ries impact event, direct evidence for the composition of the projectile is at present restricted to sub-micrometric Fe-Cr-Ni particles found in intragranular micro-fractures in the crystalline basement underlying the crater (El Goresy & Chao, 1976). On the basis of textural relationships and particles composition, the above authors suggested that the Ries impacting body was a stony meteorite. Subsequent studies (Morgan *et al.*, 1979; Pernicka *et al.*, 1987; Schmidt & Pernicka, 1994; Vennemann *et al.*, 2001) were unable to better specify the nature of the impactor.

In this framework, the finding of the unusual association of green glass including metallic spherules, never before reported in the area, may represent a new discovery of impact-related material, of paramount importance in shedding new light on the nature of the impactor generating the Steinheim-Ries craters, and may also indicate the presence of a possible, still unidentified, third impact crater.

TABLE 1 – *Stratigraphy and lithologies of Ries pre-impact target (modified from Hüttner & Schmidt-Kaler, 1999).*

| Stratigraphic Sections and Thickness (m) | Subdivisions and Lithologies | Thickness (m) |
|---|---|---|
| Tertiary<br>0-50 | Middle Miocene = sands with minor clay and limestone | 0-50 |
| Malmian<br>150-200 | ε = massive limestone<br>δ = massive limestone<br>γ = bedded limestone with some marly limestone, marl and some reef limestone<br>β = mainly bedded limestone<br>α = marly limestone, marl and bedded limestone | ~20<br>70-100<br>~30<br>~20<br>40-50 |
| Dogger<br>140-150 | γ-ζ = limestone, calcareous limestone and shale<br>β = sandstone, in part iron-rich<br>α = grey shale | ~10<br>~40<br>90-100 |
| Liassic<br>30 | Black shale with some sandstone and marl | ~30 |
| Triassic<br>250-300 | Upper Keuper = red shale<br>Middle Keuper = sandstone with some shale<br>Muschelkalk = calcareous sandstone<br>Buntsandstein | ~30<br>~200<br>0-50<br>~15 |
| Hercynian Basement | Various gneiss, granites and amphibolites | several kilometers |

An alternative possibility is that the glass derives from human activity. Sigmaringen has been known for its metallurgic activity since the 18th century, and vitreous materials are common by-products of this industrial process. Historical data report that in 1707, Meinrad II, Prince of Hohenzollern-Sigmaringen, built a blast-furnace for iron extraction in Laucherthal (near Sigmaringen), after abandoning the methods for iron forging which had long been used by his predecessors. In the following years, iron production expanded and another blast-furnace was built on the outskirts of the town. These factories were both closed in 1878, because of a financial crisis. The Hohenzollern family thought of changing type of production and, in 1890, adapted pre-existing structures to produce bronze under expert craftsmen. At the beginning of 20th century, there was a further change, when factory expansion led to the production of iron and steel.

## Analytic Techniques and Methods

Macroscopic descriptions of 80 fragments of glass (1 mm to 4.5 cm) and their metallic spherule inclusions (5 to 400 μm) were carried out at the stereo-microscope.

Subsequently, two polished thin sections (v1, v2) were obtained from one of these glass fragments (sample Sf) and studied by polarized transmitting light microscopy. Five sections of metallic spherules (1, 2, 3, 4, 5), chosen to represent sample SaX, were studied by polarized reflected light microscopy on both polished and etched surfaces.

Back-scattered electron (BSE) imaging and semi-quantitative analyses of seven glass fragments (samples Sa1, Sa2, Sa3, Sf, Sg, Be3, Bf) and metallic spherules sections (1, 2, 3, 4, 5) were performed with a scanning electron microscope (SEM, Camscan MX2500, fitted with energy dispersive spectrometer) at the Dipartimento di Mineralogia e Petrologia, University of Padova.

X-ray powder diffraction (XRPD) analyses were performed on a Philips X'Pert Pro diffractometer, with CuKα radiation and a generator setting of 40 kV and 40 mA, at the Dipartimento di Mineralogia e Petrologia, University of Padova.

Chemical analyses of glass (v1, v2) and of micro-spherules (1, 2, 3, 4, 5) were performed at the CNR–IGG laboratory (Padova) on a CAMECA Camebax Microbeam electron microprobe (EMP) fitted with four wavelength-dispersive spectrometers and one energy-dispersive spectrometer. For glass analyses, the system was operated at an accelerating voltage of 15 kV and a beam current of 15 nA. A series of natural (wollastonite for Si and Ca; corundum for Al; orthoclase for K; albite for Na) and synthetic standards ($Fe_2O_3$ for Fe; $MnTiO_2$ for Ti and Mn; MgO for Mg; $Cr_2O_3$ for Cr) were employed. For micro-spherule analyses, the system was operated at an accelerating voltage of 20 kV and a beam current of 20 nA. A series of natural pure element standards was employed.

## Description of samples and chemical composition

### *Glass*

About 80 distinct fragments of glass (1 mm to 4.5 cm) were primarily studied and photographed under the stereo-microscope. All fragments are angular and show conchoid fractures. The glass is transparent; its colour is bottle-green in most cases, except for one reddish-brown (Bg4) and seven smoke-grey (Sa3, Sa7, Sa14, Sa48, Sf, Bf, Bg2) samples. The green colour appears in a shade that is typical of moldavite (Fig. 2). Colour intensity depends on glass thickness. Almost all samples include round empty bubbles, ranging from a few μm to 0.5 cm in size. They may have chaotic distribution or be arranged along sub-parallel preferential lines (Fig. 3). Three samples (Sa1, Sa2, Sa9) have thin tubes arranged in fans along radial directions, terminating with a small spherical cavity, some of which include a metallic spherule. These tubular structures range from a few μm to about 4 mm long, and are only a few microns thick. Metallic spherules, ranging in size from 10 to 400 microns, are observed in all samples.

Seven glass fragments (Sa1, Sa2, Sa3, Sf, Sg, Be3, Bf) representing both bottle-green and smoke-grey samples were studied by SEM. They all show sets of sub-parallel conchoid fractures, have spherical cavities and contain frequent metallic spherules. The glass appears compositionally homogeneous. Cavities are generally empty, with smooth surfaces, and only occasionally include metallic spherules.

a) b)

Fig. 2 – Morphologic and chromatic aspects of studied glass samples compared with moldavite tektites. a) Sample Bf (~2.6 × 0.9 cm); b) Millimetric fragments of moldavite.

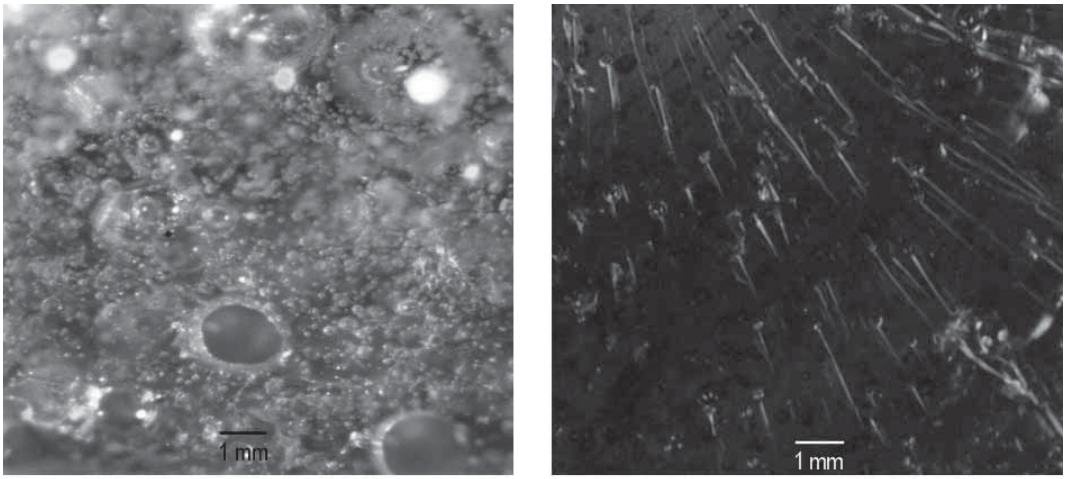


a) b)

Fig. 3 – a) Chaotic distribution of spheroid bubbles in sample Sa19; b) Thin tubes arranged in fan along radial directions and terminating with small spherical cavities.

The latter are disseminated within the glass and may be as small as one micron.

Two polished thin sections (v1,v2) were obtained from bottle-green glass fragment Sf (Fig. 4), one of the samples that most resembles moldavite glass. Under the microscope, the vitreous mass appears colourless and completely isotropic. Two zones (defined by dashed lines in Fig. 4) are characterised by up to 100μm sized aggregates of individuals of a crystalline phase. The grains are arranged in sub-parallel bands. Grains are colourless when in small crystals but have an overall greyish colour when in aggregates. Individual grains have rectangular to square outlines, with a fine skeletal aspect (locally

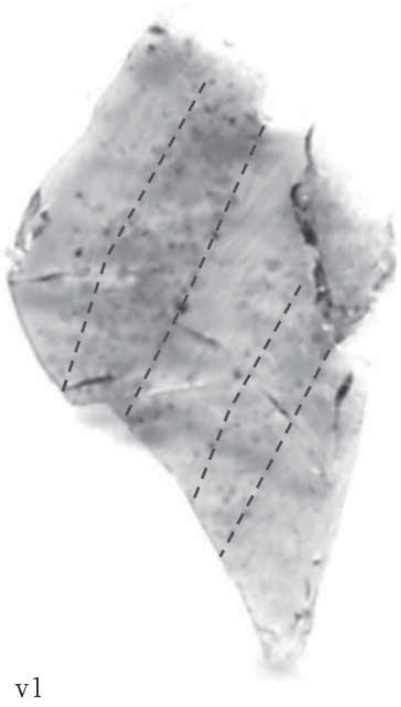


Fig. 4 – Thin section of sample Sf (v1). Dashed lines approximately define area of crystalline phases (image size: ~2.1 × 1.1 cm).

resembling snowflake structures), indicative of rapid growth. The refractive indexes of the crystalline phase are higher than those of the glass. The crystalline phase shows straight extinction, 1st order blue maximal interference colour, and hourglass zoning. It is uniaxial, with a negative optical sign and a positive sign of elongation. The overall optical properties of this phase match those of gehlenite.

Electron microprobe analyses, mean values, and standard deviations of glass and crystalline phase are listed in Tabs. 2 and 3. Glass (Tab. 2) appears fairly homogeneous and is mainly composed of $SiO_2$ (34.32 to 37.50 wt.%), CaO (31.94 to 37.50 wt.%) and $Al_2O_3$ (22.55 to 26.9 wt.%). $TiO_2$ (1.27 to 1.83 wt.%), MnO (0.56 to 0.92 wt.%), MgO (0.42 to 0.85 wt.%), $K_2O$ (0.49 to 0.98 wt.%) and FeO (0.11 to 0.35 wt.%) are present as minor components. Traces of $Cr_2O_3$ and $Na_2O$ were also detected.

Due to the small dimension and skeletal shape of the crystalline phase, only seven spots were found suitable for microprobe analysis (Tab. 3). The phase is a CaO (29.82 wt.%), $Al_2O_3$ (22.4 wt.%) silicate ($SiO_2$ = 40.70 wt.%) with minor quantities of $TiO_2$ (2.5 wt.%) and MnO (1 wt.%), and only traces of MgO, $K_2O$, FeO, $Cr_2O_3$ and $Na_2O$. Low analytical totals (from 99.22 to 96.4) may indicate the presence of undetected light components (eg., OH).

This chemical composition of the crystalline phase does not match that of gehlenite (Tab. 3). We therefore used X-ray powder diffraction to identify the phase. A diffraction pattern (Fig. 5) was obtained from 1- to 10-micron sized powder, prepared by grinding a small chip of sample Sf. Due to the dominant presence of glass and minor amount of the crystalline phase, a long time scan (60 seconds × 0.02 theta) was used in order to detect significant peaks (see details in caption). The strongest peaks ($2\theta$ = 31.42; $2\theta$ = 52.10; $2\theta$ = 29.14, $2\theta$ = 44.39) correspond well to a phase with the structure of gehlenite. The remaining peaks ($2\theta$ = 44.68; $2\theta$ = 65.03, $2\theta$ = 82.34) (Fig. 5) correspond to an iron phase with spatial group Im-3m and represent the small metallic spherules scattered within the glass.

*Metallic spherules*

Samples of metallic spherules were supplied both as loose individuals (Fig. 6) and as clusters of inclusions bound within glass fragments. Apart from their higher concentration, these metal inclusions are identical to the rarer metallic microspherules scattered in all the examined glass fragments. The spherules have a silver colour with iridescent metallic lustre. In the most cases their surface is smooth and only occasionally wrinkled. For minerographic and compositional studies, five metallic spherules (150 - 240 μm) were selected among the largest grains, mounted on epoxy, and abraded until their equatorial section was reached. Under polarized reflected light, all five appear to be homogeneous, with only slight indications of a possible second component. Secondary electron imaging carried out on one of the spherules (Fig. 7), shows two interconnected main domains. In both cases, Fe is the only element revealed by EDS analyses. One domain is apparently homogeneous; the other is composed of a mix of alternate strips

TABLE 2 – *Electron microprobe analyses (oxides wt.%) of two distinct samples of glasses (v1, v2). Each sample shows homogeneous composition and both have almost identical composition. Cumulative average (cum. av.) and standard deviation of all analysed spots are reported in the last column. Very low value of standard deviation for all elements confirms compositional homogeneity of glass.*

| | v1 | | | | | | | | | | | | | | |
|---|---|---|---|---|---|---|---|---|---|---|---|---|---|---|---|
| | 1 | 2 | 3 | 4 | 6 | 7 | 9 | 11 | 13 | 14 | 15 | 16 | 17 | 18 | 19 |
| $SiO_2$ | 35.68 | 36.03 | 36.63 | 36.50 | 36.07 | 35.12 | 36.33 | 37.50 | 35.96 | 36.07 | 36.44 | 35.85 | 36.29 | 34.32 | 35.92 |
| $TiO_2$ | 1.45 | 1.44 | 1.52 | 1.59 | 1.52 | 1.82 | 1.46 | 1.44 | 1.45 | 1.46 | 1.50 | 1.53 | 1.51 | 1.46 | 1.51 |
| $Al_2O_3$ | 25.70 | 25.31 | 25.66 | 25.52 | 25.13 | 24.89 | 25.71 | 25.08 | 25.39 | 25.01 | 25.83 | 25.30 | 25.13 | 25.15 | 25.69 |
| FeO | 0.15 | 0.33 | 0.12 | 0.12 | 0.23 | 0.22 | 0.24 | 0.11 | 0.16 | 0.28 | 0.18 | 0.23 | 0.13 | 0.13 | 0.35 |
| MgO | 0.62 | 0.61 | 0.68 | 0.61 | 0.61 | 0.77 | 0.62 | 0.42 | 0.64 | 0.66 | 0.57 | 0.64 | 0.65 | 0.62 | 0.67 |
| $Cr_2O_3$ | 0.00 | 0.10 | 0.07 | 0.03 | 0.02 | 0.12 | 0.07 | 0.09 | 0.00 | 0.13 | 0.00 | 0.04 | 0.05 | 0.02 | 0.07 |
| MnO | 0.84 | 0.76 | 0.81 | 0.81 | 0.82 | 0.69 | 0.84 | 0.84 | 0.78 | 0.75 | 0.77 | 0.92 | 0.78 | 0.74 | 0.84 |
| CaO | 32.98 | 32.82 | 32.95 | 32.59 | 32.97 | 34.01 | 33.06 | 34.76 | 33.34 | 33.37 | 32.92 | 33.26 | 32.96 | 32.38 | 33.26 |
| $Na_2O$ | 0.01 | 0.04 | 0.05 | 0.06 | 0.02 | 0.11 | 0.00 | 0.03 | 0.05 | 0.05 | 0.00 | 0.01 | 0.03 | 0.07 | 0.03 |
| $K_2O$ | 0.55 | 0.61 | 0.61 | 0.59 | 0.67 | 0.49 | 0.60 | 0.98 | 0.57 | 0.59 | 0.58 | 0.63 | 0.65 | 0.63 | 0.64 |
| Total | 97.98 | 98.05 | 99.10 | 98.42 | 98.06 | 98.23 | 98.94 | 101.25 | 98.36 | 98.37 | 98.79 | 98.41 | 98.18 | 95.52 | 98.97 |

| | v2 | | | | | | | | | | | | | | | |
|---|---|---|---|---|---|---|---|---|---|---|---|---|---|---|---|---|
| | 20 | 21 | 22 | 23 | 24 | 27 | 29 | 30 | 31 | 32 | 33 | 34 | 35 | 36 | cum. av. | *s.d.* |
| $SiO_2$ | 36.50 | 35.26 | 36.07 | 35.15 | 36.00 | 35.45 | 36.80 | 35.96 | 36.77 | 37.25 | 35.82 | 36.19 | 37.05 | 36.46 | 36.12 | *0.67* |
| $TiO_2$ | 1.51 | 1.55 | 1.42 | 1.65 | 1.51 | 1.27 | 1.47 | 1.56 | 1.50 | 1.83 | 1.49 | 1.56 | 1.47 | 1.53 | 1.52 | *0.11* |
| $Al_2O_3$ | 25.42 | 24.22 | 25.34 | 25.39 | 25.01 | 25.33 | 26.03 | 25.39 | 25.87 | 22.55 | 25.35 | 25.37 | 26.22 | 25.29 | 25.34 | *0.65* |
| FeO | 0.23 | 0.30 | 0.12 | 0.17 | 0.30 | 0.24 | 0.18 | 0.20 | 0.15 | 0.20 | 0.15 | 0.21 | 0.19 | 0.19 | 0.20 | *0.07* |
| MgO | 0.62 | 0.68 | 0.66 | 0.73 | 0.63 | 0.73 | 0.48 | 0.66 | 0.59 | 0.85 | 0.65 | 0.64 | 0.65 | 0.62 | 0.65 | *0.08* |
| $Cr_2O_3$ | 0.11 | 0.07 | 0.02 | 0.04 | 0.17 | 0.13 | 0.07 | 0.04 | 0.06 | 0.03 | 0.07 | 0.08 | 0.04 | 0.04 | 0.06 | *0.04* |
| MnO | 0.89 | 0.78 | 0.75 | 0.68 | 0.79 | 0.56 | 0.91 | 0.85 | 0.77 | 0.67 | 0.82 | 0.89 | 0.77 | 0.79 | 0.78 | *0.08* |
| CaO | 33.80 | 33.82 | 31.94 | 35.52 | 33.58 | 35.25 | 32.17 | 33.21 | 33.40 | 34.31 | 33.11 | 33.49 | 33.13 | 33.35 | 33.51 | *0.81* |
| $Na_2O$ | 0.02 | 0.03 | 0.04 | 0.06 | 0.02 | 0.03 | 0.01 | 0.03 | 0.04 | 0.00 | 0.05 | 0.04 | 0.02 | 0.00 | 0.03 | *0.03* |
| $K_2O$ | 0.65 | 0.64 | 0.64 | 0.50 | 0.62 | 0.59 | 0.67 | 0.65 | 0.62 | 0.66 | 0.60 | 0.61 | 0.61 | 0.65 | 0.63 | *0.08* |
| Total | 99.75 | 97.35 | 97.00 | 99.89 | 98.64 | 99.59 | 98.78 | 98.55 | 99.77 | 98.35 | 98.12 | 99.08 | 100.17 | 98.92 | 98.63 | |

of two components and has the typical structure of pearlite, the eutectic phase made of alternate ferrite and cementite. Etching with Nital (5% nitric acid in ethanol) was carried out to better characterize the structure, and possibly the components, of the spherules. Instead, on the etched surface (Fig. 8), spherule mainly appears to be composed of homogeneous ferrite, interconnected with areas of eutectic pearlite and eutectic steadite. Small graphite lamellae are also observed.

Electron microprobe analyses of 27 spots on the 5 metallic micro-spherules are listed in Tab. 4. The chemical compositions of two low-Ni iron meteorites are listed in Tab. 5 for comparison. Because of the close micrometric scale interconnection among the components, electron microprobe analyses of pure end-members were obtained only in a few cases. Pure ferrite was analysed in spherules 2 (spot 11), 3 (spots 17 and 19), 4 (spots 21 and 22) and 5 (spot 28). The best analyses of eutectic steadite are represented by high-P spots 12 and 13 in spherule 2 and spots 14, 16 and 18 in spherule 3. The systematic low totals of these analyses are consistent with the presence of C, an unmeasured component. The remaining spots, ranging from Fe ca. 98.5 to 87.5 and with totals as low as 87.5, very probably represent mixed analyses of the main components, with the contribution, in some cases, of pure C from graphite.

Table 3 – *Electron microprobe analyses and crystal-chemical formula of crystalline silicate phase within glass. Low standard deviation (s.d.) indicates that phase is homogeneous. The chemical composition and crystal-chemical formula of stoichiometric gehlenite is reported in the last column for comparison. Crystal-chemical formula was calculated on the basis of seven oxygen atoms.*

| | XX 5 | 8 | 10 | 12 | 25 | 26 | 28 | av. | *s.d.* | geh. |
|---|---|---|---|---|---|---|---|---|---|---|
| $SiO_2$ | 39.80 | 41.33 | 40.96 | 40.55 | 40.83 | 40.51 | 40.88 | 40.69 | *0.48* | 21.91 |
| $TiO_2$ | 2.71 | 2.33 | 2.66 | 2.27 | 2.75 | 2.08 | 2.61 | 2.49 | *0.26* | |
| $Al_2O_3$ | 22.89 | 23.05 | 22.67 | 22.95 | 21.53 | 22.15 | 21.53 | 22.40 | *0.66* | 37.18 |
| FeO | 0.13 | 0.16 | 0.30 | 0.07 | 0.21 | 0.25 | 0.14 | 0.18 | *0.08* | |
| MgO | 0.22 | 0.27 | 0.25 | 0.23 | 0.26 | 0.24 | 0.16 | 0.23 | *0.04* | |
| $Cr_2O_3$ | 0.04 | 0.11 | 0.09 | 0.12 | 0.12 | 0.05 | 0.00 | 0.07 | *0.05* | |
| MnO | 1.03 | 1.09 | 1.08 | 0.99 | 1.12 | 0.93 | 1.10 | 1.05 | *0.07* | |
| CaO | 29.13 | 29.87 | 29.41 | 29.02 | 30.46 | 30.50 | 30.35 | 29.82 | *0.64* | 40.90 |
| $Na_2O$ | 0.09 | 0.04 | 0.01 | 0.01 | 0.07 | 0.00 | 0.02 | 0.03 | *0.03* | |
| $K_2O$ | 0.39 | 0.98 | 1.05 | 0.87 | 1.06 | 0.82 | 1.04 | 0.89 | *0.24* | |
| Total | 96.42 | 99.22 | 98.49 | 97.09 | 98.41 | 97.54 | 97.84 | 97.86 | | 99.99 |
| | | | | | | | | | | |
| Si | 1.774 | 1.795 | 1.794 | 1.795 | 1.799 | 1.796 | 1.808 | 1.794 | | 1.000 |
| Ti | 0.091 | 0.076 | 0.088 | 0.076 | 0.091 | 0.069 | 0.087 | 0.083 | | |
| Al IV | 0.135 | 0.129 | 0.119 | 0.129 | 0.110 | 0.135 | 0.105 | 0.123 | | 1.000 |
| Al VI | 1.067 | 1.051 | 1.052 | 1.068 | 1.008 | 1.022 | 1.018 | 1.041 | | 0.999 |
| Cr | 0.001 | 0.004 | 0.003 | 0.004 | 0.004 | 0.002 | 0.000 | 0.002 | | |
| $Fe^{2+}$ | 0.005 | 0.006 | 0.011 | 0.003 | 0.008 | 0.009 | 0.005 | 0.007 | | |
| Mn | 0.039 | 0.040 | 0.040 | 0.037 | 0.042 | 0.035 | 0.041 | 0.039 | | |
| Mg | 0.015 | 0.017 | 0.016 | 0.015 | 0.017 | 0.016 | 0.011 | 0.015 | | |
| Ca | 1.391 | 1.390 | 1.380 | 1.376 | 1.438 | 1.448 | 1.438 | 1.409 | | 1.999 |
| Na | 0.008 | 0.003 | 0.001 | 0.001 | 0.006 | 0.000 | 0.002 | 0.003 | | |
| K | 0.022 | 0.054 | 0.059 | 0.049 | 0.060 | 0.046 | 0.059 | 0.050 | | |
| Sum | 2.548 | 2.566 | 2.562 | 2.554 | 2.582 | 2.579 | 2.574 | 2.566 | | 2.998 |
| Total | 4.548 | 4.566 | 4.562 | 4.554 | 4.582 | 4.579 | 4.574 | 4.566 | | 5.000 |

## Discussion and Conclusion

We compare here the chemical composition of glasses found in the Sigmaringen area with both moldavite and impact melts. We also examine the structure and composition of metallic spherules and compare their features with those of metallic micro-meteorites and iron meteorites.

### *Glass*

Fig. 9 describes variations in major elements with $SiO_2$ for the Sigmaringen glasses (diamonds), a selection of suevite glasses (circles) and representative moldavite glasses (square). We report here only those suevite glass compositions which are most similar to the Sigmaringen glasses. Impact suevite glasses with more silicic compositions are omitted. Crosses represent the composition of the crystalline phase observed in Singmaringen glasses, and triangles in $Al_2O_3$ and CaO diagrams represent the composition of a stoichiometric gehlenite. In all the diagrams, the different glasses define distinct areas, with no region of overlap. Among glasses, those found in Sigmaringen have the lowest $SiO_2$ contents and the highest $Al_2O_3$, CaO and $TiO_2$ contents. They show no compositional relationships with either suevite glasses or moldavite.

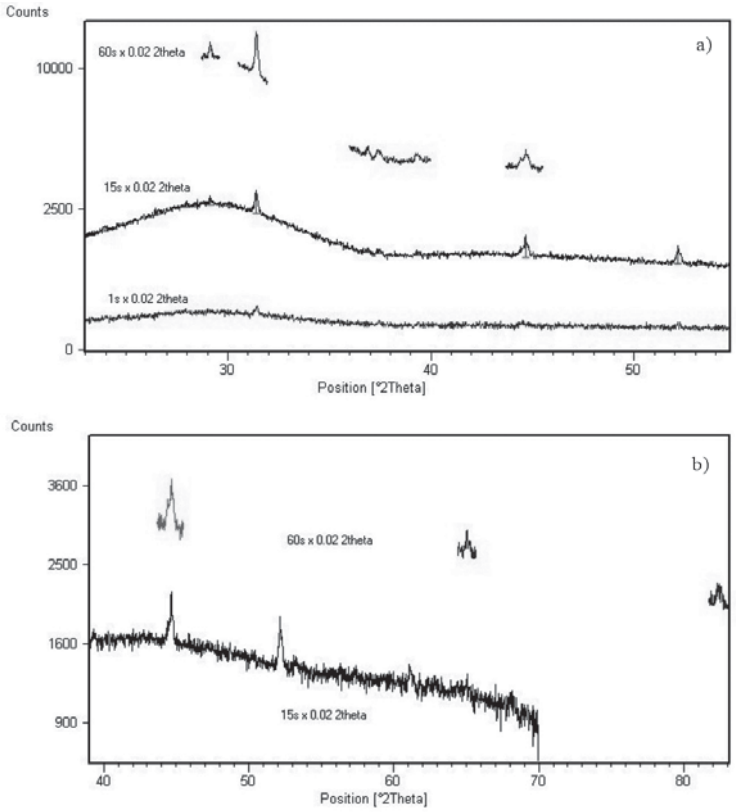


Fig. 5 – X-ray powder diffraction patterns. a) Three different scan speeds are shown. Scan 1 (bottom) had a scan speed of 1 second for each advancement step (each step is 2 hundredth of 2θ). Scan 2 (middle) had a scan speed of 15 seconds for each advancement step. Speed of scan 3 was 60 seconds for each advancement step to highlight larger relative intensity peaks of gehlenite. b) Pattern range between 40 and 85° 2θ reveals characteristic intensity peaks of iron.

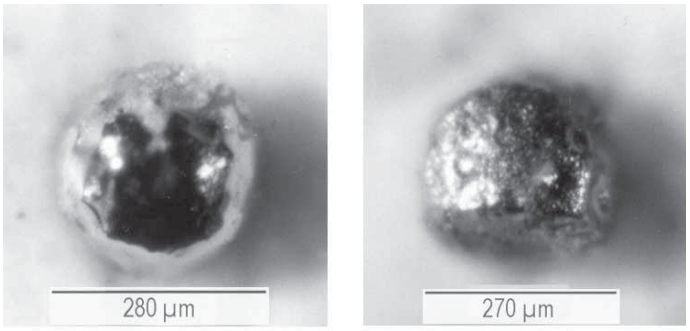


Fig. 6 – Metallic spherules. a) ~280µm sized spherule with a homogeneous, mainly smooth surface; b) ~270µm sized spherule with an extremely wrinkled surface.

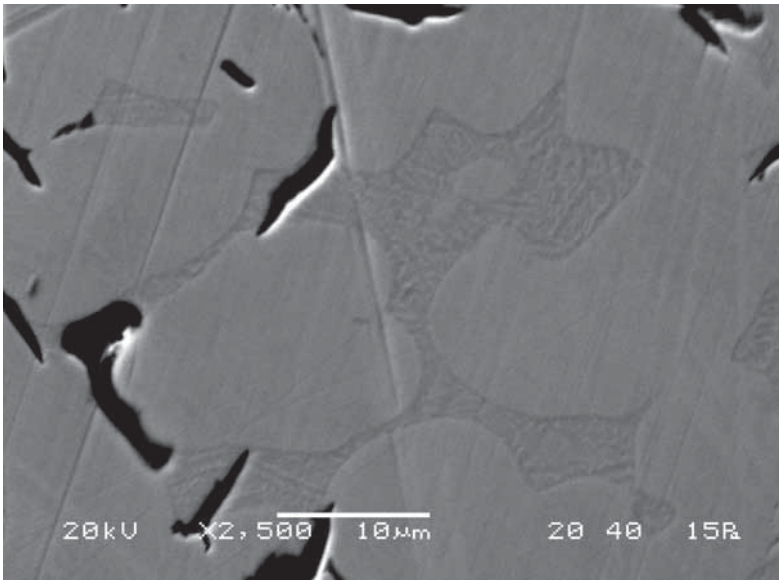


Fig. 7 – Back-scattered electron image of a metallic spherule. Two interconnected domains are evident: one is homogeneous, and one composed of a mix of alternate strips of two components, with the typical structure of pearlite, the eutectic phase of alternate ferrite and cementite. EDS analyses of both domains reveal Fe as only component. Difference in mean atomic weight of the two areas, resulting in different brightness within the picture, is thus expected to reflect the presence of a light undetected element, such as C.

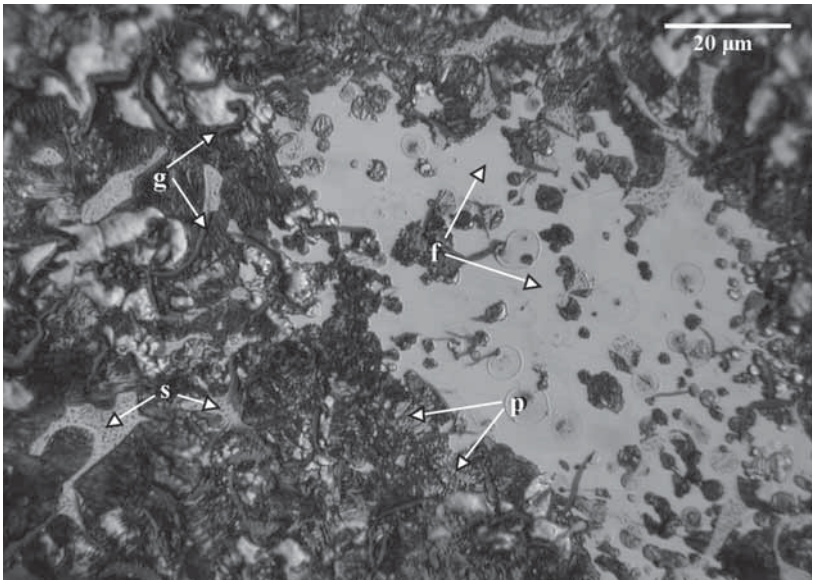


Fig. 8 – Etched surface of a metallic spherule. Spherule appears mainly composed of bright areas of homogeneous ferrite (f) interconnected with dark areas of eutectic pearlite (p) and bright, finely dotted areas of eutectic steadite (s). Small graphite lamellae (g) are also visible.

Table 4 – *Chemical composition of five distinct spherules (1, 2, 3, 4, 5) reported as elements %.*

| | 1 | | | | | | 2 | | | | | |
|---|---|---|---|---|---|---|---|---|---|---|---|---|
| | 1 | 2 | 3 | 4 | 5 | 6 | 8 | 9 | 10 | 11 | 12 | 13 |
| Fe | 95.62 | 94.62 | 97.08 | 87.48 | 89.67 | 96.71 | 98.34 | 98.29 | 93.54 | 99.58 | 87.63 | 89.20 |
| P | 0.00 | 0.00 | 0.03 | 0.00 | 0.00 | 0.00 | 0.00 | 0.00 | 0.00 | 0.00 | 9.47 | 7.34 |
| Si | 0.00 | 1.79 | 1.59 | 0.00 | 1.90 | 1.98 | 0.01 | 0.00 | 0.01 | 0.00 | 0.03 | 0.01 |
| S | 0.00 | 0.02 | 0.07 | 0.01 | 0.11 | 0.00 | 0.01 | 0.02 | 0.00 | 0.02 | 0.28 | 0.24 |
| Cr | 0.03 | 0.05 | 0.05 | 0.06 | 0.04 | 0.03 | 0.05 | 0.05 | 0.08 | 0.06 | 0.02 | 0.01 |
| Mn | 0.12 | 0.07 | 0.14 | 0.14 | 0.14 | 0.16 | 0.01 | 0.00 | 0.01 | 0.02 | 0.00 | 0.02 |
| Ni | 0.06 | 0.04 | 0.02 | 0.06 | 0.05 | 0.04 | 0.03 | 0.05 | 0.01 | 0.03 | 0.07 | 0.08 |
| Co | 0.00 | 0.00 | 0.00 | 0.00 | 0.00 | 0.00 | 0.00 | 0.00 | 0.00 | 0.00 | 0.00 | 0.00 |
| Total | 95.83 | 96.58 | 98.99 | 87.76 | 91.92 | 98.93 | 98.45 | 98.42 | 93.65 | 99.71 | 97.50 | 96.90 |

| | 3 | | | | | | | 4 | | | | 5 | | | |
|---|---|---|---|---|---|---|---|---|---|---|---|---|---|---|---|
| | 15 | 17 | 19 | 20 | 14 | 16 | 18 | 21 | 22 | 23 | 24 | 26 | 27 | 28 | 29 |
| Fe | 98.62 | 99.19 | 99.05 | 96.86 | 90.02 | 89.25 | 89.77 | 99.04 | 99.00 | 98.43 | 96.91 | 94.70 | 98.02 | 99.26 | 98.67 |
| P | 0.00 | 0.26 | 0.02 | 0.30 | 8.12 | 7.25 | 7.59 | 0.48 | 0.38 | 0.90 | 1.00 | 0.76 | 0.59 | 0.77 | 0.61 |
| Si | 0.01 | 0.01 | 0.00 | 0.01 | 0.01 | 0.01 | 0.00 | 0.04 | 0.01 | 0.02 | 0.01 | 0.01 | 0.02 | 0.01 | 0.01 |
| S | 0.00 | 0.01 | 0.00 | 0.01 | 0.22 | 0.22 | 0.12 | 0.00 | 0.00 | 0.02 | 0.03 | 0.02 | 0.01 | 0.02 | 0.02 |
| Cr | 0.06 | 0.06 | 0.04 | 0.02 | 0.06 | 0.07 | 0.05 | 0.05 | 0.03 | 0.02 | 0.03 | 0.02 | 0.02 | 0.01 | 0.05 |
| Mn | 0.02 | 0.00 | 0.00 | 0.02 | 0.00 | 0.00 | 0.01 | 0.00 | 0.00 | 0.00 | 0.00 | 0.02 | 0.00 | 0.01 | 0.00 |
| Ni | 0.00 | 0.01 | 0.00 | 0.00 | 0.00 | 0.03 | 0.00 | 0.00 | 0.02 | 0.04 | 0.03 | 0.05 | 0.03 | 0.02 | 0.00 |
| Co | 0.00 | 0.00 | 0.00 | 0.00 | 0.00 | 0.00 | 0.00 | 0.00 | 0.00 | 0.00 | 0.00 | 0.00 | 0.00 | 0.00 | 0.00 |
| Total | 98.71 | 99.53 | 99.11 | 97.23 | 98.43 | 96.84 | 97.54 | 99.62 | 99.44 | 99.43 | 98.00 | 95.58 | 98.69 | 100.09 | 99.36 |

Table 5 – *Chemical analysis of low-Ni iron meteorites taken from literature (Faure, 1991; Fornaseri, 1994).*

| | Iron Meteorite 1 (Faure, 1991) | Iron Meteorite 2 (Fornaseri, 1994) |
|---|---|---|
| Fe | 90.60 | 90.20 |
| Ni | 7.90 | 8.46 |
| Co | 0.50 | 0.55 |
| P | 0.20 | 0.15 |
| S | 0.70 | 0.04 |

For the sake of discussion, it is worth noting that the composition of our glass samples have no correspondent among natural terrestrial (or extra-terrestrial) magmatic melts, and hence cannot represent a volcanic glass either.

The measured glass composition is similar, although it does not entirely correspond, to the mean compositions of common slag derived from metallurgic processes of iron ore reduction. Common slag from blast-furnace processes usually has much lower $Al_2O_3$ and higher $SiO_2$ contents. However, the glass composition closely matches one of the glass phases which may separate from molten slag during cooling. In the $CaO$ - $SiO_2$ - $Al_2O_3$ ternary diagram used for slag characterisation (Bodsworth, 1995), our glass composition plots in the field of gehlenite liquids, i.e. liquids which, while cooling, may generate a crystalline phase with gehlenite structure: a phase which was actually detected in our samples.

The high $Al_2O_3$ content is not usual in present-day slag, and may indicate early attempt in finding the most appropriate flux.

The XRD spectrum (Fig. 5) of the small dendritic crystalline phase is fully consistent with that of gehlenite and does not match any other phase. Despite this indication and the consistent optical characters the composition of the phase is significantly different from that of stoichiometric gehlenite (Tab. 3). This discrepancy cannot be ascribed to analytical problems, such as possible mixing with the surrounding glass. In fact the

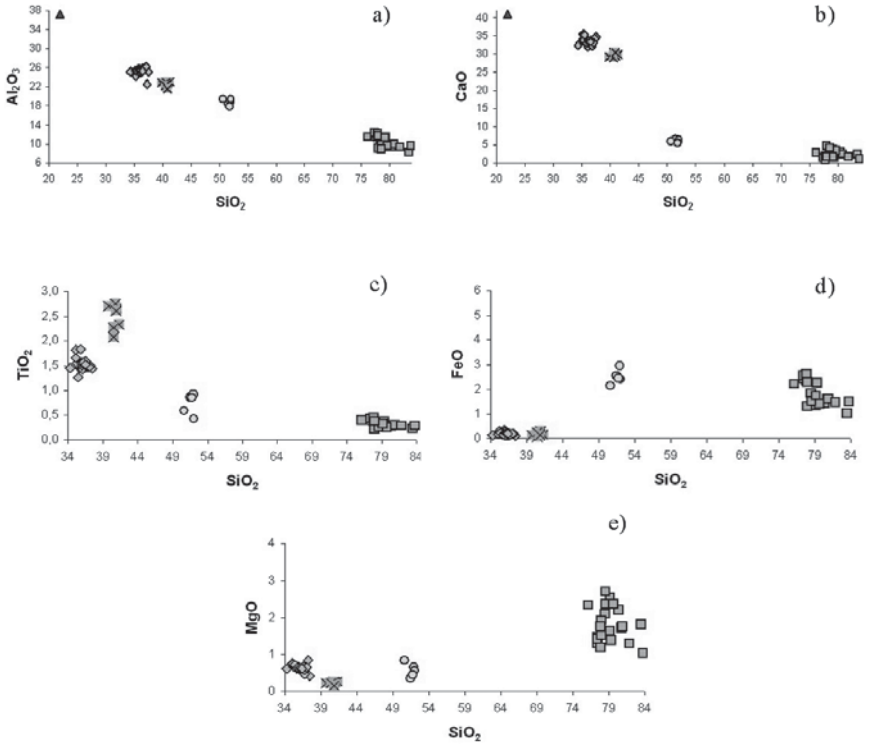


Fig. 9 (a to e) – Variation diagrams of elements vs. $SiO_2$. Diamonds: chemical composition of 29 glass analyses; crosses: chemical composition of 7 crystalline phase analyses; circles: chemical composition of suevite glass (Osinski, 2003); squares: moldavite composition (Meisel, *et al*., 1997); triangle (diagrams a and b): composition of stoichiometrich gehlenite [chemical formula: $Ca_2Al(AlSi)O_7$].

crystalline phase does not plot on the mixing line between glass and stoichiometric gehlenite. Non stoichiometry of the crystalline phase may result from the fast growth in a quenched environment.

*Metallic spherules*

Chemical data (Tab. 4) and variation diagrams of P, Ni and Co *vs*. Fe (Fig. 10) show that metallic spherules investigated in this work (circles and diamonds) significantly differ from iron meteorites (squares) due to their lack of Ni and Co. High-P iron-nickel phases are common in meteorites (eg., schreibersite $(FeNi)_3P$; barringerite $(FeNi)_2P$). The high P phase (circles) detected in the spherules is totally devoid of Ni, indicating that it is of terrestrial origin. The metallographic texture revealed by etching and the electron microprobe composition of the distinct phases are common in steel and cast iron produced in blast-furnace during iron ore reduction.

The high concentrations of silicon and manganese in the spherules exclude that they are the result of present-day, or even recent, manufacturing processes, and indicate older technological activities in the area, consistent with reduction processes of iron ore as operated 150-200 years ago.

Historical data support this conclusion quite nicely, as the Sigmaringen area has been known for its metallurgic activity since the early 18$^{th}$ century.

Although promising, the investigated materials have no relation with the Ries crater impactor, the nature of which still remains elusive. In the end, a study which was intended to shed new light on the nature of the projectile of one of the main impact

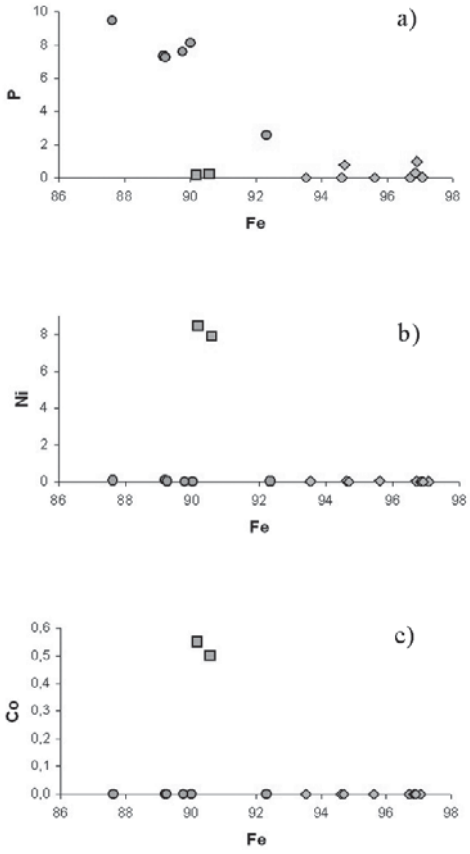


Fig. 10 (a to c) – Variation diagrams for metallic phases. Iron meteorite composition (squares) is substantially different from composition of sampled micro-spherules (circles: high P spots; diamonds: low P spots) due to systematically higher Ni and Co contents.

craters in Europe was unintentionally "derailed" towards archaeometric implications.

ACKNOWLEDGEMENTS

We dedicate this paper to the memory of Filippo Olmi. We are grateful to E. Ragazzi for involving us in this research, and to R. Carampin for his support in EMP analyses. XRD analyses and interpretations were carried out by F. Zorzi. The help of A. Guastoni and L. Peruzzo with SEM analyses is gratefully acknowledged. This paper benefited by the constructive reviews of the editor S. Menchetti, M. Mellini, and anonymous referees.

REFERENCES

BODSWORTH C. (1995) – *Physical chemistry of iron and steel manufacturing*. Longman, London.

EL GORESY A. and CHAO E.C.T. (1976) – *Discovery, origin, and significance of Fe-Cr-Ni veinlets in the compressed zone of the 1973 Ries research drill core*. Geol. Bavarica, **75**, 305-321.

ENGELHARDT W.V. (1997) – *Suevite breccia of the Ries impact crater, Germany: petrography, chemistry and shock metamorphism of crystalline rock clasts*. Meteorit. Planet. Sci., **32**, 545-554.

FAURE G. (1991) – *Principles and applications of geochemistry*. Prentice Hall, New Jersey. 600 pp.

FORNASERI M. (1994) – *Lezioni di geochimica*. Masson Editoriale Veschi, Milano. 825 pp.

FRENCH B.M. (1998) – *Traces of catastrophe: a handbook of shock-metamorphic effects in terrestrial meteorite impact structure*. LPI contribution No. 924, Lunar Planet. Inst., Houston. 120 pp.

HÜTTNER R. and SCHMIDT-KALER H. (1999) — *Erlauterungen zur geologischen Karte des Rieses 1:50000*. Geol. Bavarica, **104**, 7-76.

LANGE J.M. (1996) – *Tektite glasses from Lusatia (Lausitz), Germany*. Chem. Erde, **56**, 498-510.

LAURENZI M.A., BIGAZZI G., BALESTRIERI M.L. and BOUŠKA V. (2003) – *$^{40}Ar/^{39}Ar$ laser probe dating of the Central European tektite-producing impact event*. Meteorit. Planet. Sci., **38**, 831-967.

MEISEL T., LANGE J.-M. and KRÄHENBÜHL U. (1997) – *The chemical variation of moldavite tektites: simple mixing of terrestrial sediments*. Meteorit. Planet. Sci., **32**, 493-502.

MORGAN J.W., JANSSENS M.J., HERTOGEN J., GROS J. and TAKAHASHI H. (1979) – *Ries impact crater, southern Germany: Search for meteoritic material.* Geochim. Cosmochim. Acta, **43**, 803-815.

OSINSKI G. R. (2003) – *Impact glasses in fallout suevites from the Ries impact structure, Germany: an analytical SEM study*. Meteorit. Planet. Sci., **38**, 1641-1667.

PERNICKA E., HORN P. and POHL J. (1987) – *Chemical record of the projectile in the graded fall-back sedimentary unit from the Ries Crater, Germany*. Earth Planet. Sci. Letters, **86**, 113-121.

SCHMIDT G. and PERNICKA E. (1994) – *The determination of platinum group elements (PGE) in target rocks and fall-back material of the Nordlinger Ries impact crater, Germany*. Geochim. Cosmochim. Acta, **58**, 5083-5090.

Stöffler D. (1974) – *Deformation and transformation of rock-forming minerals by natural and experimental shock process: Physical properties of shocked minerals*. Fortsch. Mineral., **51**, 256-289.

Stöffler D., Artemieva N.A. and Pierazzo E. (2002) – *Modeling the Ries-Steinheim impact event and the formation of the moldavite strewn field*. Meteorit. Planet. Sci., **37**, 1893-1907.

Vennemann T., Marlok A., Engelhardt W.v. and Kyser K. (2001) – *Stable isotope composition of impact glasses from the Nordlinger Ries impact crater, Germany*. Geochim. Cosmochim. Acta, **65**, 1325-1336.